Modeling the dispersion of traffic-derived black carbon emissions into hilly terrain

Sameer Singh (sam166104024@iitg.ac.in)
Indian Institute of Technology Guwahati
Sharad Gokhale
Indian Institute of Technology Guwahati

Research Article

Keywords: AERMOD, Aethalometer, Black Carbon, Dispersion, Hilly terrain, Vehicular emission

Posted Date: August 1st, 2022

DOI: https://doi.org/10.21203/rs.3.rs-1901688/v1

Version of Record: A version of this preprint was published at Environmental Monitoring and Assessment on July 15th, 2023. See the published version at https://doi.org/10.1007/s10661-023-11554-6.

Abstract

This study examines hilly terrain's effect on black carbon (BC) dispersion. The apportionment of distinct sources obtained by a two-component mixing model (Aethalometer: AE-33) using improved radiative transfer equations showed the dominance of traffic-derived black carbon (BCFF) emissions in the study region. The AERMOD was used to model BC emissions from moving traffic as line source and parking lot as area source using observational and WRF-processed meteorology for the winter (Jan to Mar 2020). The model results showed that the BC levels substantially vary with local meteorological conditions, traffic volume, and composition. The hilly terrain obstructs the winds and develops a negative pressure loading to a vacuum on the other side of the hills, which promotes the accumulation of emissions, causing high BC concentrations. The pockets of higher concentration were seen at the locations where steep slopes were associated with low winds (<1 m-s−1) and hill fogs. The AERMOD model, after statistical evaluation against the observational datasets, has been applied to study the reduction in BCFF concentrations due to the implementation of Indian emission norms as mitigation measures, i.e., BS-IV (equivalent to Euro 4) and BS-VI (equivalent to Euro 6). It was found that the BCFF concentrations for BS-IV and BS-VI reduced by 35% and 75%, respectively. The model was also used to study the contribution of the different vehicular categories to BC concentration.

Highlights

- First time, the AERMOD model was employed to study the dispersion of fossil-fuel-originated black carbon into hilly terrain.
- Low wind with hill fog facilitated the rise of BC concentration in the complex terrain.
- On-site meteorological data produce more reliable dispersion calculations than WRF modeled data.
- Application of the model to study the impacts showed that traffic-derived BC for BS-IV decreased by 35% and 75% for BS-VI emission norms.

1. Introduction

Black carbon (BC) particles are one of the carbonaceous aerosols' most notable light-absorbing constituents, easily transportable vertically and horizontally over a long distance in a shorter duration (Goldberg, 1985; Ramanathan and Charmichael, 2008; Bond et al., 2013). BC aerosols are microscopic submicron particles produced from incomplete combustion of biofuel, fossil fuel, and biomass burning as a primary source (USEPA, 2012). These emitted particles are insoluble in water, while the irregular morphology facilitates the adsorption of other species in the atmospheric environment (Petzold et al., 2005). The formation of aggregates starts immediately after emission, and the aggregates get superficially or internally mixed. Therefore, hardly any pure BC particles exist in the atmosphere, particularly in a highly polluted atmosphere. The particles grow via coagulation during transport. Their size distribution is directly related to the atmospheric processes and formation mechanism during transport (Jacobson and Turco, 1995). The more efficient the fuel burn, the smaller the particles. Usually,

the BC particles are assigned to the Aitken mode, but they grow in the atmosphere due to subsequent coagulation and are found in the accumulation mode (Väkevä et al., 2002). BC has its importance in the current situation of global warming as it is the third-largest contributor that absorbs solar radiation at all wavelengths ranging from 370 to 950 nm (Ramanathan and Charmichael, 2008). It is directly allied to the ambient atmosphere through dissimilar physicochemical and biological developments disturbing local air quality (Jacobson, 2004). BC emissions in urban and suburban regions of developing countries have enlarged with commercial expansion, fast growth, daily energy demand, and open biomass burning (Liu et al., 2018). On-road traffic and industrial activities are the dominant sources of BC emissions in the Indo-Gangetic plains, Brahmaputra river basin, and Tibetan plateau (Rana et al., 2019). For example, the vehicles plying on the roads of the Indian cities are all mixed in the various proportion of Bharat Stage (BS)-II, BS-III, and BS-IV (similar to Euro 4) compliant (Singh and Gokhale, 2022). Though, the Indian government introduced BS-IV (identical to Euro 6) emission norms in April 2020 to curb the emissions from vehicular activities. Chronic exposure to BC particles associated with on-road traffic emissions may significantly reduce life expectancy and cause mortality and morbidity (WHO, 2012). The mass concentration and impacts of BC depend on the strength of the sources, local geography, and meteorological conditions of the specific region. In the atmosphere of hilly terrain emissions are trapped in the lower layer of the earth, particularly in winter than in other seasons, due to more extended hill-fog events and poor meteorological conditions (Hůnová et al., 2021). The wind flow pattern in hilly terrains is complicated with no particular direction due to high and low ridges obstructing the direct wind flow. Low wind and low-temperature cause fog to stay at a low altitude, creating a hazy environment and making particle dispersion difficult. The mountainous regions are more sensitive to weather conditions than the surroundings at lower elevations (Goldreich et al., 1986). Approximately 75% of the area in Northeast India comprises a hilly ecosystem where snow-capped small- to steep-sloped hills and valleys (less than 5 km above mean sea level) dominate the physical landscape (Singh and Gokhale, 2022). Thus, measurements and observations of BC in the hilly areas with considerable human settlements are essential to improve understanding of the impacts of BC, its contribution to total aerosol light absorption, and dispersion in hilly terrain.

Forecasting dispersion of particulate matter from a low-level source in hilly terrain is challenging mainly because of wind-flow patterns. The models such as ISCST, CALPUFF, and AERMOD are widely used for studying the dispersion of airborne pollutants (Al-Jeelani, 2013; Huang and Guo, 2019; Michanowicz et al., 2016; Tartkovasky et al., 2013; Tartkovasky et al., 2016; Vaitiekunas et al., 2007; Venkatram et al., 2009). AERMOD is the advanced Gaussian plume model (USEPA, 2018). For near-field applications (less than 50 km), it accounts for airborne pollutant impacts in flat and complex terrain within the same modeling framework (USEPA, 2018; Huang and Gao, 2019). The pollutant dispersal is Gaussian in straight and upright directions in the stable boundary layer. The terrain is a physical feature of an area involving vertical and horizontal dimensions of the land surface that tempers atmospheric processes (Hutchinson and Gallant, 1999). Huang and Gao (2019) applied the AERMOD model to simulate the dispersion of odor, hydrogen sulfide (H_2S), ammonia (NH_3), and respirable dust from a broiler, dairy, and a cage-layer barn emission in the Prairies in Canada. The model estimated the impacts of odor up to about

3 km. Tartkovasky et al. (2016) studied the dispersion of total suspended particles (TSP) and PM_{10} emissions from five stone quarries in a hilly area east of Israel's coastal plain using AERMOD CALPUFF. They found AERMOD's predictions better than those obtained by CALPUFF. A study by Al-Jeelani, (2013) of dispersion of traffic emissions of various air pollutants at Haram Mosque in Makkah, Saudi Arabia, using AERMOD, found that high-rise buildings act as flow obstacles. The AERMOD model is also applied to evaluate volatile organics from traffic emissions (Venkatram et al., 2009). Thus, AERMOD is a well-considered air pollutant dispersion model, mainly used to point sources in flat and hilly terrains (Venkatram et al., 2009; Al-Jeelani, 2013; Tartkovasky et al., 2013; Tartkovasky et al., 2016). The long-range transport and transboundary influence of aerosols originating from the Indo-Gangetic plains to the northeastern part of India are reported (Singh and Gokhale, 2021). However, the effect of geography on air pollutant dispersion and meteorological parameters is mainly unexplored.

The primary objective of this study is to investigate the dispersion of traffic-derived BC emissions in a hilly terrain through field study and modeling. This study presents the results of the AERMOD dispersion modeling of combined BC emissions originating from moving traffic as line source and parking lot as area source over the complex terrain region of northeast India using observational and WRF-processed meteorology for the winter period (Jan - Mar 2020). The AERMOD model is also evaluated against the observational BC concentrations (by AE33) in two topographical areas during winter 2020 and applied to study the reduction in BC due to the implementation of Bharat Stage emission norms BS-IV and BS-VI.

2. Materials And Methods

2.1 Sampling details and instrumentation

The data for carrying out the research has been collected in the study region for the winter season from Jan-Mar 2020 as per the standard methodology (CPCB, 2011). The study region in northeastern India is geographically located between high and low elevation topographies in the north and south, respectively. In the west to east direction, the Brahmaputra river acts as a leaking wall through which air pollutants are transported from Indo-Gangetic plains to Tibetan plateaus (Singh and Gokhale, 2021). The undulating topography with a small- to steep-slope may be limiting dispersion within the boundary. It is surrounded by eighteen hills and is a part of the Indo-Burma biodiversity hotspot. Fig. 1 shows the study area and two monitoring sites on Nilachal Hill. This hill houses many residents and is a worship place that attracts many pilgrims and vehicles.

BC's real-time measurements were conducted by a dual spot two-component mixing Aethalometer (model: AE-33, Magee Scientific Inc., Berkley, USA) model at seven discrete wavelengths near UV to near IR regions. It pumps particle-laden air at a set flow rate of two-liter min^{-1}, collects the fraction of particles on filter tape, and logged BC levels every minute. The filter tape used was TFE coated glass filter tape roll (30 mm. × 30 ft., Part No. 8050). It was operated as per the listed environment conditions in the user manual and checked periodically for appropriate flow rate, thus reducing possible measurement errors. The AE-33 model was used to segregate biomass and fossil fuel burning in the whole of BC (Sandradewi

et al., 2008). This method assumes that the optical absorption of BC at a particular wavelength ($b_{abs\_BC\_\lambda}$) is a summation of biomass and fossil fuel contributions, and the equivalent absorption coefficient follows λ^{-1} and λ^{-2} spectral dependences, respectively. While considering aerosol angstrom exponent, values 1 and 1.7 produced better results in this region (Fig. S1). Hence, BC_{FF} and BC_{BB} were calculated for a spectral band 370-880, and default mass absorption cross-section values were used as provided by the manufacturer (Drinovec et al., 2015).

A low volume fine particulate sampler (APM 550M, Envirotech Instruments Pvt. Ltd.) fitted with a $PM_{2.5}$ impactor was also deployed to gather daily 24-hr integrated $PM_{2.5}$ samples. The samples have been collected on pre-desiccated (25°C, 24 h) PTFE filters (2 µm, 46.2 mm Dia., Whatman, USA). The filters were analyzed gravimetrically using an electronic weighing balance (model: Sartorius CD-225D, Germany, sensitivity: ±0.001 mg) at constant temperature and relative humidity. These were weighted thrice before and after sampling, followed by the determination of residual mass by deducting the mean of pre-sampling weights from the mean of post-sampling weights. The change amongst the repetitive weightings was less than 16 µg.

To monitor the traffic characteristics, video recorders were installed at two locations- the parking lot area (L1) on the hilltop (26.16473°N, 91.707038°E, 225 m [asl]), Assam Trunk road (L2) in the foothills of the valley (26.159981°N, 91.70603°E, 66.83 m [asl]), and the data acquisition period was 07:00 – 20:00 each day (referred to as daily in this study). Of the 14-h measurements we attempted (686 h), data was effectively captured for 678 h (98.83%). After that, the videotapes were analyzed to determine the traffic characteristics such as hourly traffic volume, traffic flow rate, and traffic volume in different compositions. As per the Automotive Research Association of India (ARAI, 2008 & 2017), the traffic composition was classified into five different categories termed as two-wheelers (2W: motorcycles, mopeds, and scooters), three-wheelers (3W: Auto-rickshaws), four-wheelers (4W: passenger cars), light transport vehicles and mini passenger carriers (LDDV), and buses and heavy trucks (HDDV).

To observe the local meteorological conditions, a wireless weather station was (model: Vantage Pro, California, USA) installed (~1 km to the west-north-west) at Air & Noise Pollution Laboratory, Indian Institute of Technology Guwahati. It was located on the terrace of the building (~12 m high), and data were recorded at five-minute intervals. It includes atmospheric temperature (°C), wind speed (m s^{-1}), rainfall (mm), relative humidity (%), barometric pressure (mbar), wind direction (°), and solar radiation (W m^{-2}). We used meteorological records from January to March 2020 containing at least 17 days. These were the only days for which BC data was recorded around the L1 site using the Aethalometer (AE-33) model. The wind rose of each month is almost similar to their entire winter wind roses (Fig. S2). Therefore, the outcomes of this study are appropriate outside the exact dates used for which the AERMOD and Aethalometer models were studied. Precisely, the prevailing winds in the region were from the southeast. During the study period, the mean daily minimum and maximum temperatures ranged from 14.31 - 24.67°C (19.09 ± 2.74°C) and 25.3 - 28.37°C (26.91 ± 1.12°C), respectively, with an overall

rainfall of 11 mm. The mean relative humidity was the highest in January (79.27 ± 4.15%) and lowest in March (64.50 ± 9.92%), while the mean wind speed (<1.4 m/s) was almost similar.

The entire setup mentioned above was synchronized daily to ensure the data's quality. All the instruments were equipped with a backup power supply, which powered them for nearly 15 minutes during the electricity interruption period.

2.2 Emission rate calculation for AERMOD modeling

Emission factors are highly variable and depend on the combustion engine's technology and particulate reduction equipment fitted out in automobiles (Bond et al., 2004; Myung and Park, 2011; Yan et al., 2011). BS-IV (~Euro 6) and BS-VI (~Euro 4) emission norms were implemented in 2017 and 2020, respectively, in India to reduce emissions from vehicles fitted with direct gasoline injection and compression ignition or diesel engines. It is important to note that BS-VI norms are applicable to all categories of vehicles all over India. At the same time, a significant fraction of the traffic fleet is comprised of the vehicles of BS-II, BS-III, and BS-IV vehicles. Many autos in the city have two-stroke engines. Its results are not yet realized as the penetration of BS-VI vehicles is in a negligible fraction. The adopted Emission factors were obtained from Paliwal et al. (2016), which developed the emissions at the district level. It was spatially dispersed onto the grids at a resolution of 40×40 km^2 (Table 1). The emissions (in mg/s) were calculated for both the adopted and the proposed emission norms by equation 1.

$$EF_w = \frac{\sum_{j=1}^{n} N_j \times EF(i,j) \times ATS}{N_{vehicles}} \quad (1)$$

where EF_w, N_j, EF (i,j), and $N_{vehciles}$ denote the weighted emission factor (mg s^{-1}), the number of vehicles of an individual category, the emission factor of pollutant i for a j^{th} vehicle category, respectively. The average traffic speed (ATS) for the traffic fleet of 20 km hr^{-1} is analyzed from the videotapes.

2.3 Structure for AERMOD model

The modeling measures firmly tailed the Indian Air Quality Modeling Guidelines (CPCB, 1998). The presence of obstacles (e.g., slight to steep slopes and building heights) significantly influences the meteorological conditions (e.g., wind field) and dispersion pattern of air pollutants. Hence, three primary data inputs were prepared to run the AERMOD model: vehicular emission rate, atmospheric data (temperature, wind speed, cloud cover, wind direction, relative humidity, mixing height, precipitation, pressure), and topography data (altitude, hills and valleys elevation). The AERMOD modeling system has two modules, AERMET- to process the meteorology to produce the meteorological data contours for both observed and WRF processed met data, and AERMAP- to process the terrain data to create the

topography data contours for identified receptors. Composed with vehicular emission rates, the outputs of these two modules were incorporated into the third section, AERMOD- to produce BC concentration contours at the receptors in the modeling domain for the specified interval.

At two geographical locations (L1 and L2), variation in the daily vehicular count was observed, suggesting that varying emission rates need to be used instead of static values. The road traffic at L1 was considered congested since the vehicles were stopped at the parking lot area. Furthermore, the road traffic at L2 was considered free-flowing to account for a variable emission since, during congestion, emission may be constant. L1 and L2 were treated as an area and line source types, respectively. The L2 location had the highest daily-average traffic volume, much higher than L1 (Table S1). However, on weekend days at the L1, more traffic was seen. The average class-wise traffic contribution at L1 and L2 locations is shown in Fig. S3. The L1 site is 225 degrees to the north of the monitoring station. Many small vendors' stalls, shops, a health center, and residential houses are located near this station. Many people, thus, may be exposed to higher levels of traffic-related air pollutants. The share of BC in $PM_{2.5}$ from fossil fuel (BC_{FF}) sources was found to be 11% (ranging from 6-20%) (Fig. 2b). Based on these findings, the BC emission rates were derived from ARAI (2017). 2W and 4W vehicles were considered gasoline engines; hence the fraction (BC_{FF} in $PM_{2.5}$) is taken as 6%. Similarly, 3W, LDDV, and HDDV vehicles were considered diesel engines; the fraction is taken as 20%. The emissions were estimated for each hour, day, month, and winter season using the emission rates listed in Table 1. The background concentration of BC_{FF} was obtained as the 1.25^{th} percentile of the observed BC concentration from the whole dataset (Kondo et al., 2006), i.e., ~3 μg m^{-3}. This concentration is used as a boundary concentration in AERMOD calculations of the contribution from local urban sources.

Two sets of weather data were used as inputs to the AERMOD model in this study- data from a Weather Station (observed met data) and Weather Research Forecasting model (WRF)-produced onsite meteorological data (modeled met data). AERMOD model assumes that concentrations at all distances during a modeled period are governed by the temporal-average meteorology of the period. The observed and the modeled met data, including surface meteorological conditions and upper air sounding records, were used for the dispersion modeling. These data were processed in the AERMET that generated two meteorological data profiles for AERMOD modeling. In the observed met data, cloud cover is needed by the weather-related preprocessor AERMET for generating the input records. Though, cloud cover is barely recorded in typical weather-related stations. Specifically, actual solar radiation (in W m^{-2}) at a specific period is measured in the meteorological station at Air & Noise Pollution Laboratory, IIT Guwahati. However, cloud cover was not available. Hence we used equation 2 to derive the cloud cover (Kasten and Czeplaks, 1980; Kim and Hofmann, 2005).

$$SR = SR_0(1 - 0.75\, c^{3.4}) \quad (2)$$

where SR and SR_o (units in W m^{-1}) denote the solar radiation under cloudy/actual/real-time and clear sky situations, separately. c denotes the cloud cover (0 to 1). Precisely, the peak value amongst the quantities in each month is presumed to signify solar radiation during clear sky situations, while the value at a specific hour on the day is presumed to denote the real-time solar radiation situations in the simulated period. The Upper air estimator tool of the AERMET view was used to approximate the upper-air parameters. The reason for using onsite meteorological data was to compare the obtained results that were processed using WRF data, which may still provide valuable results. We have also used the meteorological data from the pollution control board (PCB) located at 7 km in the southeast-south.

The topography may cause acceleration, deceleration, and refraction of wind arrangements to a significant level (Hunova et al., 2021). Complex topography produces limited-scale movements of air pollutants. The Shuttle Radar Topography Mission of one Arc-second (SRTM1) data at ~30 m resolution was used in the domain's AERMAP module. Currently, SRTM is a thorough in elevation resolution digital topographic catalogue of Earth (Tartakovasky et al., 2016). Terrain elevations were in meters relative to the mean sea level built on the WGS84 coordinate system, Zone 46R, which varied from 44 to 354 m in the specified domain. A buffer of 10 m was considered from the predefined extent of the modeling domain for proximity analysis. The AERMAP was utilized to formulate the topography info built on the source locations, SRTM data, and receptor locations.

For receptor locations in the complex terrain, the modeling process employed a Cartesian receptor grid with 100 m receptor spacing, in addition to two discrete receptors. The Cartesian receptor grid varied as per modeling extent. The modeling extent was 1050 x 1350 m from SW coordinates (26.157508°N, 91.701921°E). The 154 receptors excluding L1 and L2 locations were defined in the modeling domain, each with a different height due to uneven terrain heights.

To determine the best modeling estimates for the study domain few constraints were used, which were found to be realistic conditions to conduct the modeling studies. These constraints were:

1. Estimation of BC_{FF} concentrations at locations L1 and L2 using mean background BC concentration as a boundary condition at the monitoring location.
2. Estimation of BC_{FF} concentrations using daytime (07:00 am – 08:00 pm local time) emission rate at the monitoring location as background concentration.
3. Estimation of BC_{FF} concentrations in a bowl-shaped topography only to reveal the obstruction in BC dispersion that could occur due to uneven terrain.

To conduct an AERMOD modeling study under these conditions, a traffic volume study was conducted at two unlike locations L1 and L2. Due to the unavailability of data at nighttime, the model prediction was performed for the specified time.

2.4 Statistical parameters for AERMOD evaluation

Due to the effect of arbitrary atmospheric developments, there may not be any flawless model in air quality modeling (Chang and Hanna, 2004). The Model operational efficiency can be evaluated by relating the modeled and observed concentration of the pollutants using appropriate statistical measures. Hanna, (1993) recommended the usage of numerical performance methods such as fractional bias, geometric mean bias, geometric variance, correlation coefficient, and the fraction of extrapolations within a factor of two observations, normalized mean square error, and index of the agreement for testing the performance of air quality models as listed in Table 2. The performance of AERMOD was also quantitatively evaluated using specific multiple out of sample cross-validation and external validation methods (Willmott, 1985; Hanha et al., 1988; Hanna et al., 1993; Keller et al., 2014). Cross-validation was assessed using two measures termed root mean square error (RMSE) and cross-validation R^2 (R_{CV}^2) (Keller et al., 2014). For each period, BC concentrations were estimated at the monitoring site L1. The index of association, covariation, or correlation between observed and estimated concentrations measures the strength of model predictions. The Pearson product-moment correlation (r), the proportion of variance explained by estimated BC concentrations, and R are standard statistical indicators. It is also common to find r or R's statistical significance to corroborate the correlation coefficient's interpretation (Willmott, 1985).

3. Results

Figure 2 displays the daily diurnal variation of $PM_{2.5}$ and the fraction of fossil fuel associated BC in $PM_{2.5}$ during the study period. The daily mean observed BC_{FF} mass concentration ranged from 3.11 to 16.29 μg m^{-3} (mean: 7.09 ± 2.62 μg m^{-3}). BC_{FF} concentration was peaked during morning rush hour (09:00 LST), and the lowest was observed in the late afternoon (15:00 LST). It might be attributed to the emissions and the complex terrain. The weighted fraction of BC_{FF} in $PM_{2.5}$ varied from 0.06 to 0.20 (maxima). It should be noted that the daily (24 hr) mean BC_{FF} and $PM_{2.5}$ mass concentrations were used to estimate the fraction of BC_{FF} in $PM_{2.5}$.

The winter averaged BC_{FF} contour is displayed in Fig. 3. Each contour comprises all receptors under a similar BC_{FF}. Consequently, from the contours, dissimilar BC_{FF} dispersion expanses can be resolute to a certain level.

Figure 4 shows the comparison of the observed and the modeled concentrations at L1. The model underestimated the BC_{FF} concentrations by ~ 12% and better simulated the higher values. The R^2 value was 0.71 (Fig. S4). BC_{FF} concentrations were found to be much higher than those reported in other parts of the country (Fig. S5).

Figure 5a displays the application of the AERMOD model for the evaluation of BS-IV and BS-VI implementation. The results showed apparent reductions in BC_{FF} concentrations due to improved emission factors. It also shows the variation in emission rates according to the traffic volume and vehicle category at two locations, L1 and L2 (Fig. 5b and 5c).

4. Discussion

The rising levels of BC from fossil fuel combustion are usually concerned with ambient air quality and public health (WHO, 2012). In the present study, the AERMOD model was utilized to conclude the effect of complex terrain on BC_{FF} dispersion for a region of Guwahati, India. The aim was to study source-meteorology-terrain interactions and their combined effects on BC dispersion using the AERMOD model. The impact of traffic on air quality was studied. This study was directed to validate if BC concentrations at setback distances are impacting human health during long-term and short-term exposure. There are no regulations or standards on ambient air quality to control the BC_{FF} or BC concentration. WHO recommended BC concentration limits of 20 μg m^{-3} for annual BC. In the following discussion, all possible directions were considered. The aim was to quantify the winter influence and relate winter average BC_{FF} contours with dispersion happening frequency contours.

As for winter average BC_{FF} contours, very low BC_{FF} concentration limits (as small as 0.2 μg m^{-3}) were selected to plot BC_{FF} dispersion travel expanses because average winter BC_{FF} above 0.9 μg m^{-3} presented very short dispersion distances (< 100 m) and even BC_{FF} of 0.2 μg m^{-3} simply had an extreme length of ~ 300 m. The farthest BC_{FF} dispersion occurred in the north, while it was the shortest in the east. This may be due to the wind mostly blowing from the southwest direction, and the terrain in the west direction hinders the dispersion of BC_{FF}. The winter wind rose demonstrates that the main winds in the valley are from the SE, and the wind speed is typically less than 1.5 m s^{-1}. Hence, BC_{FF} is getting accumulated in the valley. Comparing the two monitoring locations, the impact areas are evidently unlike, with the highest spreading influence area anticipated for the L2 location tailed by the L1 location primarily due to the difference in the emission rates. Considering BC_{FF} of 0.2 μg m^{-3}, the maximum dispersal is up to 120 m for the L1 location and 50 m for the L2 location. As numerous factors affect BC_{FF} dispersal in the ambient environment, it is hard to point out the causes for such a significant change of the two locations to one factor. Though, a plentiful higher emission rate and geographical region for L2 location should be the primary purpose to clarify its considerably greater impact region.

Epidemiological studies deliver adequate proof of the link between cardiopulmonary mortality and morbidity with exposure to BC (Janssen et al., 2011; WHO, 2012). Toxicological studies recommend that BC may act as a common carrier of a wide range of substances of erratic harmfulness to the mortal group. Though BC may not be a significant, straight lethal constituent of fine particulate substance ($PM_{2.5}$), reducing people's contact with particulate material containing BC may mitigate its effects on their well-being, as well as facilitate to reduce of climate change. AERMOD simulation revealed that the terrain facilitates the trapping of ambient BC concentrations, and their effects are limited to very few meters as per terrain elevations.

The performance of the AERMOD model was quantitatively validated by comparing it with the observed BC concentrations using statistical measures (Table 2). In order to evaluate the performance of AERMOD, the statistical parameters mentioned in section 2.5 were calculated for daily averaged observed and

modeled BC_{FF} concentrations. We observed good overall agreement between the different methods. The statistics as shown in Table 2. It can be observed that the model satisfies the statistical requirements (FB, NMSE = 0.0, and GMB, GV, R, FAC2 = 1.0). The winter model (targeted only winter season) produced significant prediction accuracy R^2_{CV} = 0.64. Michanowicz et al. (2016) found higher AERMOD model prediction accuracies by using cross-validated in summer (0.65) in comparison to winter (0.52) for $PM_{2.5}$ concentrations. The index of agreement value was 0.91, which is within the range of recommended parameter value.

Two hypothetical scenarios were tested following BS-IV and BS-VI emission standards with all vehicles. The results showed apparent reductions in the BC_{FF} concentrations due to improved emission factors (Fig. 5a). The decrease in the BC_{FF} concentrations for BS-IV and BS-VI were 35% and 75%, respectively. Further, the vehicle-category-wise contributions to the BC_{FF} concentrations were estimated. It was found that 4-W and 2-W gasoline vehicles were the top contributors to the ambient BC_{FF} concentration despite significantly lower emission factors compared to the diesel vehicles (Table 1). The collective effect of large numbers of 2W and 4W vehicles was the significant share of ambient BC_{FF} concentration (Fig. 5b and 5c). The higher emission rates for HDDV vehicles account for their almost equal share compared to LDDV and 3W categories. The diesel-driven vehicles (3W, LDDV, and HDDV), with less traffic volume (than gasoline vehicles) and high emission factors, impacted BC_{FF} air quality. Therefore, the adoption of the emission norms by diesel vehicles may fetch immediate environmental benefits. Implementing the recommended BS-VI radiation criteria will fundamentally bring Indian motor automobile guidelines into an alliance with European Union (EU) regulations for LDDV, 2W, and commercial vehicles, for example, buses and heavy-duty trucks. Four and two-wheelers had a high impact due to the high share in the traffic fleet, while 3W, LDDV, and HDDV had a high impact due to higher emissions rates. Hilly terrain obstructs the winds and creates a vacuum on the other side of the hills, promoting BC accumulation, and causing high BC concentrations. This accumulation of pollutants may increase personal exposure for those living in the valley. The variation in the spatial distribution was less on foggy days. The evaluation of AERMOD with the observed data demonstrated its predictive ability over complex terrain. The model was also applied to BC pollution reduction due to the implementation of BS-IV and BS-VI. Above all, the WRF modeled wind field delivered poorer quality dispersal approximations than using atmospheric observations from the locations positioned at 1 km ahead of the radiation sources.

5. Conclusions

The meteorological pattern in hilly regions produces a complicated dispersion pattern of pollutants or spatial distribution of pollutants mainly due to the variable height of hills. Therefore, in this study, on-site meteorology was used in the AERMOD model to estimate the BC concentration from traffic emissions which were compared with the WRF meteorology in the model. It was found that the on-site meteorology-modeled BC matched well with the observed BC as compared with the WRF meteorology-modeled BC. The spatial distribution of BC in the domain was variable because of the accumulation of BC at specific locations due to moderate- to steep-sloping hills. After verifying the model's performance, it was applied

to estimate the current scenario and the scenario produced after implementing BS-IV (equivalent to Euro-IV) and BS-VI (equivalent to Euro-VI). It was found that BS-IV reduced BC by 35% and BS-VI by 75%.

Declarations

Acknowledgments

This study has been funded by the Science and Engineering Research Board (SERB) of the Department of Science & Technology (DST), Government of India (Grant Number: EMR/2014/001039). We also gratefully acknowledge the Air and Noise Pollution Research Laboratory of the Indian Institute of Technology Guwahati, India for providing the necessary data and support.

References

Al-Jeelani, H.A., 2013. The impact of traffic emission on air quality in an urban environment. Journal of Environmental Protection, 4, 205-217.

ARAI, T., 2008. Emission factor development for Indian vehicles. *India: The Automotive Research Association of India*.

Automotive Research Association of India (ARAI), 2017. 47th annual report (https://araiindia.com/cpanel/Files/NEW_4242018123327PMWebsite_version-_ARAI__Annual_Report_2016-17.pdf).

Bond, T.C., Doherty, S.J., Fahey, D.W., Forster, P.M., Berntsen, T., DeAngelo, B.J., Flanner, M.G., Ghan, S., Kärcher, B., Koch, D. and Kinne, S., 2013. Bounding the role of black carbon in the climate system: A scientific assessment. *Journal of geophysical research: Atmospheres*, *118*(11), 5380-5552.

Bond, T.C., Streets, D.G., Yarber, K.F., Nelson, S.M., Woo, J.H. and Klimont, Z., 2004. A technology-based global inventory of black and organic carbon emissions from combustion. *Journal of Geophysical Research: Atmospheres*, *109*(D14).

Chang, J.C. and Hanna, S.R., 2004. Air quality model performance evaluation. *Meteorology and Atmospheric Physics*, *87*(1), 167-196.

CPCB, (1998). Assessment of Impact to Air Environment: Guidelines for Conducting Air Quality Modelling. ISBN: 81-86396-96-9 (http://www.cpcbenvis.nic.in).

Drinovec, L., Močnik, G., Zotter, P., Prévôt, A.S.H., Ruckstuhl, C., Coz, E., Rupakheti, M., Sciare, J., Müller, T., Wiedensohler, A. and Hansen, A.D.A., 2015. The" dual-spot" Aethalometer: an improved measurement of aerosol black carbon with real-time loading compensation. *Atmospheric Measurement Techniques*, *8*(5), 1965-1979.

Goldberg, E.D., 1985. Black carbon in the environment: properties and distribution.

Goldreich, Y., Druyan, L.M. and Berger, H., 1986. The interaction of valley/mountain winds with a diurnally veering sea/land breeze. *Journal of climatology*, *6*(5), 551-561.

Hanha, S.R., 1988. Air quality model evaluation and uncertainty. *Japca*, *38*(4), 406-412.

Hanna, S.R., 1993. Uncertainties in air quality model predictions. In *Transport and Diffusion in Turbulent Fields* (pp. 3-20). Springer, Dordrecht.

Huang, D. and Guo, H., 2019. Dispersion modeling of odour, gases, and respirable dust using AERMOD for poultry and dairy barns in the Canadian Prairies. *Science of The Total Environment*, *690*, 620-628.

Hůnová, I., Brabec, M., Malý, M., Dumitrescu, A. and Geletič, J., 2021. Terrain and its effects on fog occurrence. *Science of The Total Environment*, *768*, 144359.

Hutchinson, M.F. and Gallant, J.C., 1999. Representation of terrain. *Geographical information systems*, *1*, 105-124.

Jacobson, M.Z. and Turco, R.P., 1995. Simulating condensational growth, evaporation, and coagulation of aerosols using a combined moving and stationary size grid. *Aerosol science and technology*, *22*(1), 73-92.

Jacobson, M.Z., 2004. Climate response of fossil fuel and biofuel soot, accounting for soot's feedback to snow and sea ice albedo and emissivity. *Journal of Geophysical Research: Atmospheres*, *109*(D21).

Kasten, F., Czeplak, G., 1980. Solar and terrestrial radiation dependent on the amount and type of cloud. Solar Energy 24, 177-189.

Keller, T., Berli, M., Ruiz, S., Lamandé, M., Arvidsson, J., Schjønning, P. and Selvadurai, A.P., 2014. Transmission of vertical soil stress under agricultural tyres: Comparing measurements with simulations. *Soil and Tillage Research*, *140*, 106-117.

Kim, H.C. and Hofmann, E.E., 2005. Evaluation and derivation of cloud-cover algorithms for calculation of surface irradiance in sub-Antarctic and Antarctic environments. *Antarctic Science*.

Kondo, Y., Komazaki, Y., Miyazaki, Y., Moteki, N., Takegawa, N., Kodama, D., Deguchi, S., Nogami, M., Fukuda, M., Miyakawa, T. and Morino, Y., 2006. Temporal variations of elemental carbon in Tokyo. *Journal of Geophysical Research: Atmospheres*, *111*(D12).

Liu, Y., Yan, C. and Zheng, M., 2018. Source apportionment of black carbon during winter in Beijing. *Science of the Total Environment*, *618*, 531-541.

Michanowicz, D.R., Shmool, J.L., Tunno, B.J., Tripathy, S., Gillooly, S., Kinnee, E. and Clougherty, J.E., 2016. A hybrid land use regression/AERMOD model for predicting intra-urban variation in PM2. 5. *Atmospheric*

environment, *131*, 307-315.

Myung, C.L. and Park, S., 2012. Exhaust nanoparticle emissions from internal combustion engines: A review. *International Journal of Automotive Technology*, *13*(1), 9.

Paliwal, U., Sharma, M. and Burkhart, J.F., 2016. Monthly and spatially resolved black carbon emission inventory of India: uncertainty analysis. *Atmospheric chemistry and physics*, *16*(19), 12457-12476.

Petzold, A., Schloesser, H., Sheridan, P.J., Arnott, W.P., Ogren, J.A. and Virkkula, A., 2005. Evaluation of multiangle absorption photometry for measuring aerosol light absorption. *Aerosol science and technology*, *39*(1), 40-51.

Ramanathan, V. and Carmichael, G., 2008. Global and regional climate changes due to black carbon. *Nature geoscience*, *1*(4), 221-227.

Rana, A., Jia, S., and Sarkar, S. (2019). Black carbon aerosol in India: A comprehensive review of current status and future prospects. *Atmospheric Research*, 218(111), 207–230.

Sandradewi, J., Prévôt, A.S.H., Weingartner, E., Schmidhauser, R., Gysel, M. and Baltensperger, U., 2008. A study of wood burning and traffic aerosols in an Alpine valley using a multi-wavelength Aethalometer. *Atmospheric Environment*, *42*(1), 101-112.

Singh, S. and Gokhale, S., 2021. Source apportionment and light absorption properties of black and brown carbon aerosols in the Brahmaputra River valley region. *Urban Climate*, *39*, 100963.

Singh, S. and Gokhale, S., 2022. Effect of COVID-19 epidemic-led lockdowns on aerosol black carbon concentration, sources and its radiation effect in northeast India. *Journal of Earth System Science*, *131*(2), 1-14.

Tartakovsky, D., Broday, D.M. and Stern, E., 2013. Evaluation of AERMOD and CALPUFF for predicting ambient concentrations of total suspended particulate matter (TSP) emissions from a quarry in complex terrain. *Environmental Pollution*, *179*, 138-145.

Tartakovsky, D., Stern, E. and Broday, D.M., 2016. Dispersion of TSP and PM10 emissions from quarries in complex terrain. *Science of the Total Environment*, *542*, 946-954.

USEPA (2012). Report to Congress on Black Carbon Department of the Interior, Environment, and 153 Related Agencies Appropriations Act, 2010. Technical Report March, U.S. Environmental Protection Agency.

USEPA, 2018. AERMOD Implementation Guide. EPA-454/B-21-002. U.S. Environmental Protection Agency, Research Triangle Park, North Carolina 27711.

Vaitiekūnas, P. and Banaityte, R., 2007. Modeling of motor transport exhaust pollutant dispersion. *Journal of Environmental Engineering and Landscape Management*, *15*(1), 39-46.

Väkevä, M., Kulmala, M., Stratmann, F. and Hämeri, K., 2002. Field measurements of hygroscopic properties and state of mixing of nucleation mode particles. *Atmospheric Chemistry and Physics*, *2*(1), 55-66.

Venkatram, A., Isakov, V., Seila, R. and Baldauf, R., 2009. Modeling the impacts of traffic emissions on air toxics concentrations near roadways. *Atmospheric Environment*, *43*(20), 3191-3199.

Willmott, C.J., Ackleson, S.G., Davis, R.E., Feddema, J.J., Klink, K.M., Legates, D.R., O'donnell, J. and Rowe, C.M., 1985. Statistics for the evaluation and comparison of models. *Journal of Geophysical Research: Oceans*, *90*(C5), 8995-9005.

World Health Organization, 2012. *Health effects of black carbon*. WHO.

Yan, F., Winijkul, E., Jung, S., Bond, T.C. and Streets, D.G., 2011. Global emission projections of particulate matter (PM): I. Exhaust emissions from on-road vehicles. *Atmospheric Environment*, *45*(28), 4830-4844.

Abbreviations

BC: Black Carbon; BS: Bharat Stage; BC_{FF}: Black Carbon associated with fossil fuel combustion; ATS: Average Traffic Speed; CPCB: Central Pollution Control Board.

Tables

Tables 1-2 are available in the supplementary files section.

Figures

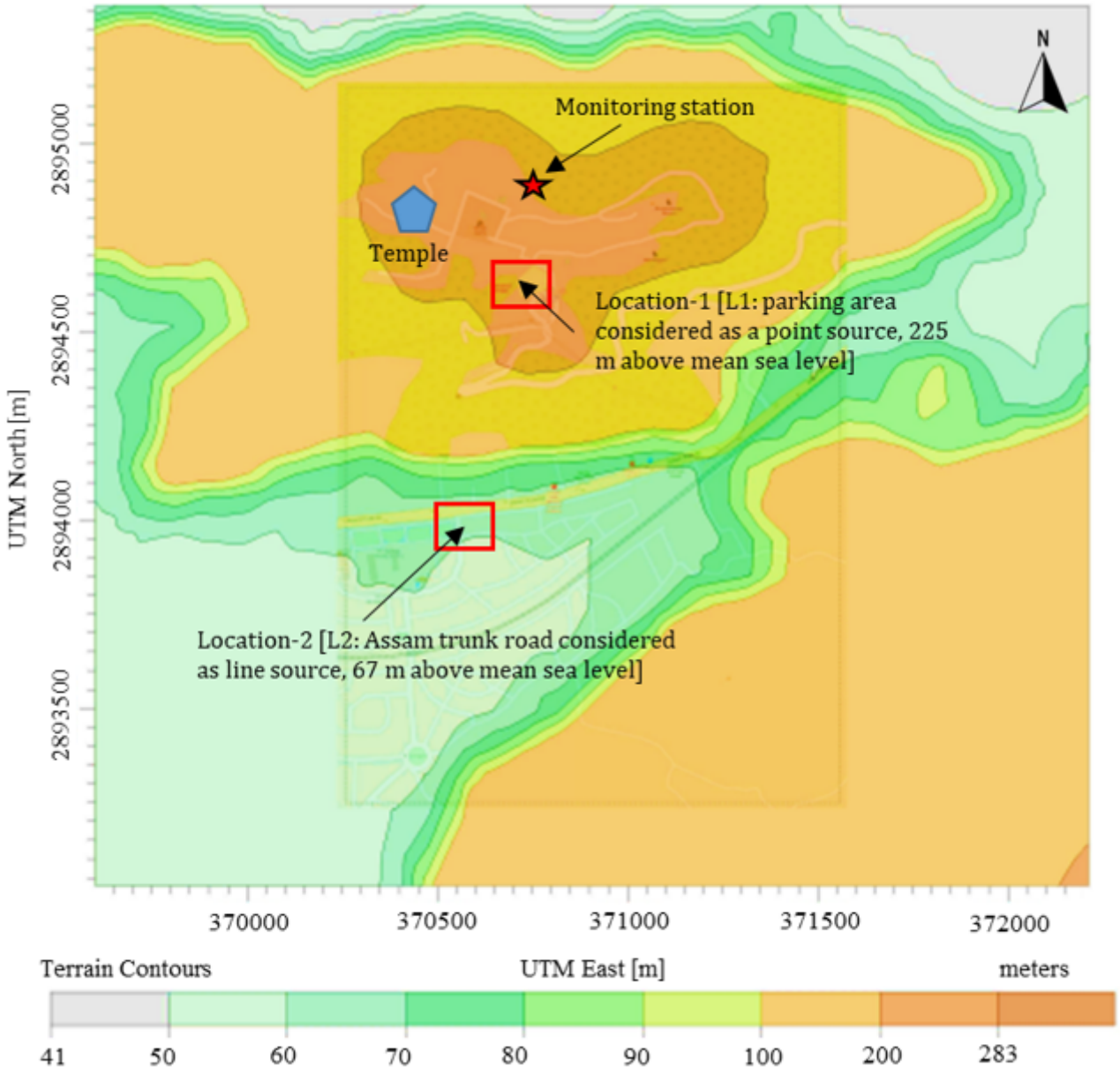

Figure 1

The details of the monitoring locations in India's modeling domain.

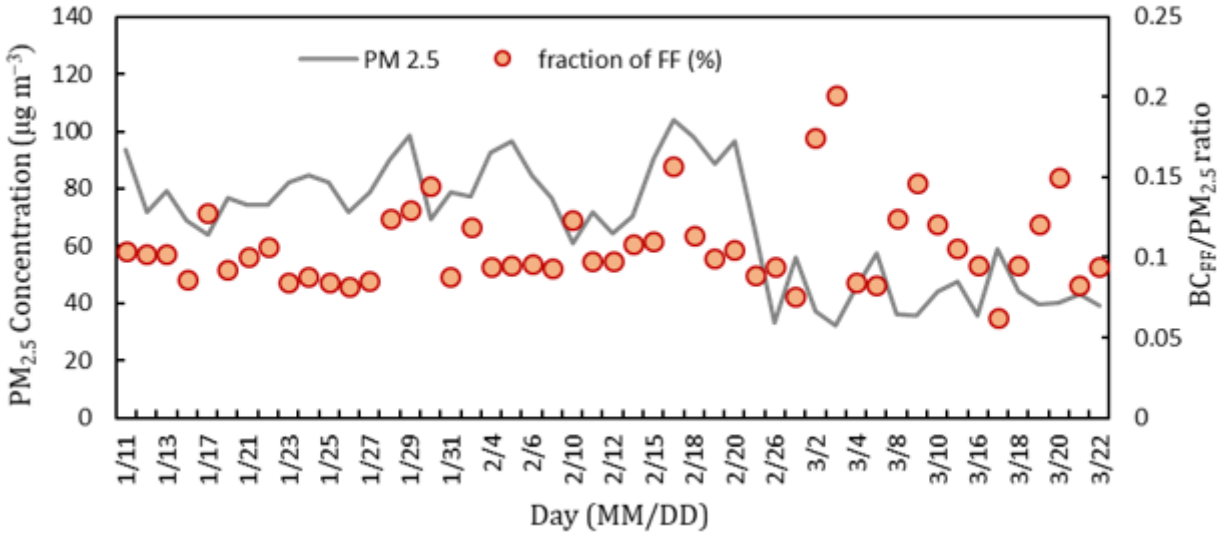

Figure 2

Diurnal variation of the $PM_{2.5}$ concentrations and the fraction of fossil fuel burning BC in $PM_{2.5}$ for the winter season.

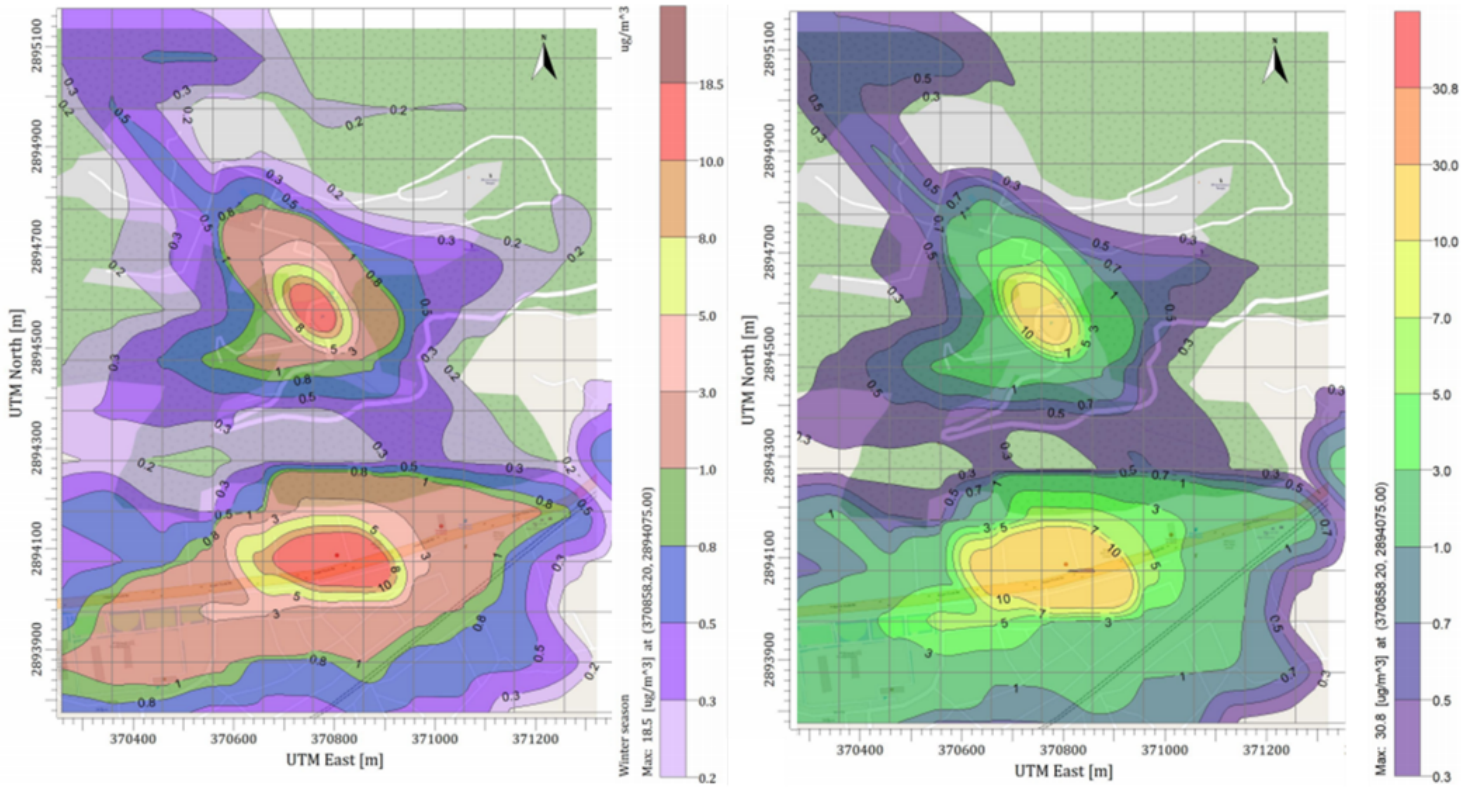

Figure 3

Contour plots of BC mass concentration using AERMOD model (a) for the whole period and (b) for the 9th highest hour.

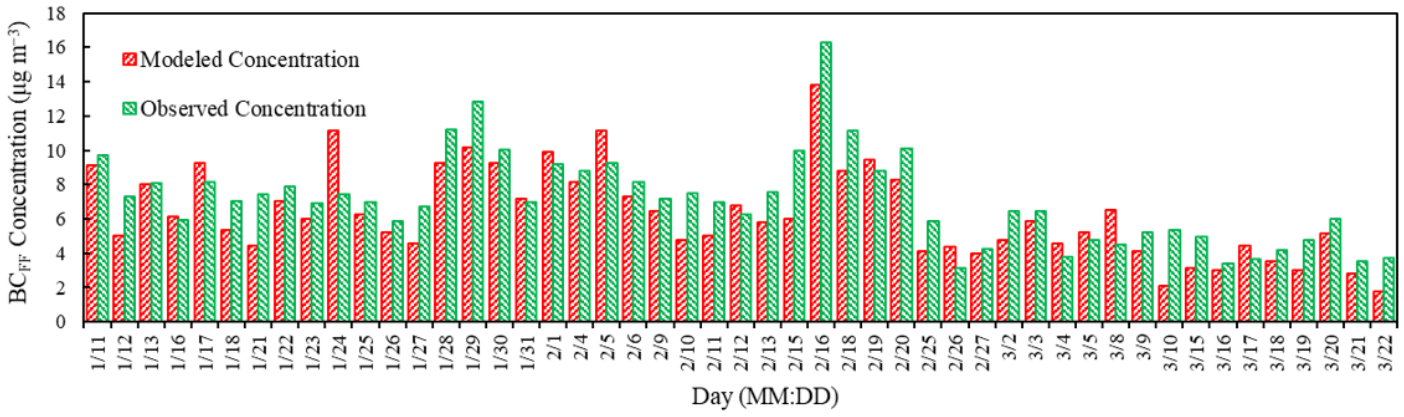

Figure 4

Comparison of observed (Aethalometer) and modeled (AERMOD) BC_{FF} mass concentrations at location L1.

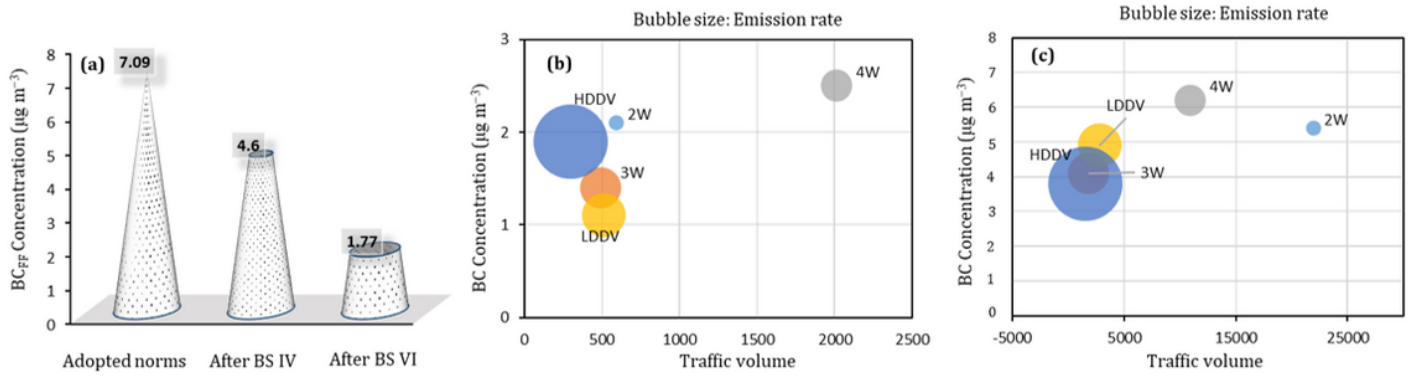

Figure 5

(a) Evaluation of BS-IV and BS-VI standards implementation, Bubble plot showing class variations in emission rate, volume, and related BC_{FF} emission at (b) L1 and (c) L2 locations, respectively.

Supplementary Files

This is a list of supplementary files associated with this preprint. Click to download.

- Table.docx
- Supplimentaryfile.docx